(Received 13 May 2024, Accepted 29 July 2024, Scheduled 12 August 2024)

An Eight-Element MIMO Antenna System Supporting Dual Bands for 5G Mobile, FSS, and DBS Communication

Raj Kumar Mistri[1,3], Ajit Kumar Singh[1], Santosh Kumar Mahto[1], Rashmi Sinha[2], Khaled Alhassoon[4], Ahmed Jamal Abdullah Al-Gburi[5,*], and Mohd Muzafar Ismail[5,*]

[1]*Department of Electronics and Communication Engineering, Indian Institute of Information Technology Ranchi 834010, Jharkhand, India*
[2]*Department of Electronics and Communication Engineering, National Institute of Technology Jamshedpur 831014, Jharkhand, India*
[3]*Department of Electronics and Communication Engineering, RTC Institute of Technology, Ranchi 835219, Jharkhand, India*
[4]*Department of Electrical Engineering, College of Engineering, Qassim University, Buraydah 52571, Saudi Arabia*
[5]*Center for Telecommunication Research & Innovation (CeTRI) Fakulti Teknologi dan Kejuruteraan Elektronik dan Komputer (FTKEK) Universiti Teknikal Malaysia Melaka (UTeM) Jalan Hang Tuah Jaya, Durian Tunggal, Melaka 76100, Malaysia*

ABSTRACT: This article presents an 8×8 Multiple-Input Multiple-Output (MIMO) antenna system that operates in two frequency bands: 3.4–3.8 GHz and 10.5–14.0 GHz. The core element of this antenna system is a rectangular patch with a line slot. To assess the diversity performance of this MIMO antenna, various parameters like S-Parameters, Envelope Correlation Coefficient (ECC), Mean Effective Gain (MEG), Channel Capacity Loss (CCL), Total Active Reflection Coefficient (TARC), and Channel Capacity (CC) were used. The study demonstrates a strong alignment between measurement and simulation results. The article thoroughly analyzes the simulated and measured performances of the lower band (LB) (3.4–3.8 GHz) and upper band (UB) (10.5–14.0 GHz). In the LB, the measured values for parameters such as reflection coefficient, mutual coupling coefficient, TARC, total efficiency, ECC, MEGi-MEGj, CCL, and CC all surpass or equal specific benchmarks. Specifically, these values are better than -6 dB, 10 dB, -11 dB, 56%, 0.15, 0.83 dB, 0.275 bps/Hz, and 38 bps/Hz, respectively. For the UB, the values are also quite favorable, exceeding or closely matching key criteria: -6 dB, 10 dB, -5 dB, 40%, 0.2, 1.6 dB, 0.55 bps/Hz, and 33.6 bps/Hz. These findings suggest that the intended MIMO antenna meets the necessary conditions for both the LB and UB regions. As a result, it appears to be a promising choice for applications in 5G mobile networks and satellite communications, including Direct Broadcast Satellite (DBS) and Fixed Satellite Services (FSS).

1. INTRODUCTION

To minimize the effects of multipath obstruction and enhance system capacity, MIMO antenna technology is widely used [1]. It is well known that smartphones employing massive MIMO arrays typically use six to eight antenna units that operate in the sub-6 GHz bands [2]. It has also been reported that the calculated upper bound of channel capacity for an eight-element MIMO system can reach up to 46 bps/Hz in a Rayleigh fading channel with a 20-dB signal-to-noise ratio (SNR), which is about four times the upper bound of channel capacity (11.5 bps/Hz) for a conventional 2×2 MIMO system [3]. In today's era, incorporating numerous antenna units in a mobile phone with extremely limited space presents an exceedingly challenging task, although it is known that MIMO technology can efficiently enhance spectrum capacity and data bit rate. To optimize isolation and spectrum efficiency in tightly packed multiple antenna arrangements in a MIMO system for 5G communication, decoupling techniques, and most importantly, the simple and compact shape of the antenna unit become fundamental needs for future antenna design. Recently, various MIMO antennas [4–13] have been developed for sub-6 GHz (5G mobile/laptop) applications operating on single frequency bands. A hybrid structure comprising a C-shaped coupled feed (symmetrically positioned about the midpoint of the long edges of the system substrate) and an L-shaped monopole slot (symmetrically positioned about the corner), along with a common square loop for an antenna pair with two individually connected feeding strips, has been reported. This antenna element structure, operating in the frequency band of 2.55–2.65 GHz [4, 5], achieves orthogonal polarization, which minimizes coupling properties between antennas and improves MIMO capacity.

The operating frequency for [6–10] is 3.5 GHz, specifically in the band 3.4–3.6 GHz. In these studies, the employed antenna structures include a bent monopole and an edge-fed dipole that form an antenna pair, two asymmetrical replicated gap-coupled loop antennas relative to the ground plane, a symmetrically placed dual L-structured radiating element with a T-structured feeding component, a composition of UL-structured radiating components with two extra longitudinal stubs and a T-

* Corresponding authors: Ahmed Jamal Abdullah Al-Gburi (ahmedjamal@ieee.org); Mohd Muzafar Ismail (muzafar@utem.edu.my).

structured feeding component, and a composition of an open-end slot antenna including a tuning stub fed by an inverted-L structured microstrip line, respectively. In [11], the antenna unit (operating in the frequency band 3.3–3.6 GHz) features two different shapes: one is a slot including a coupled feed structure, and the other is a monopole structure. The element structure in [12] consists of inverted L-structured elements and parasitic L-structured strips extending from the ground plane, operating within the frequency band 3.3–3.7 GHz. The element structure in [13] includes an L- or inverted-L-shaped microstrip feed line with a rectangular clearance and an open slot in the ground plane, operating within the frequency band 3.4–3.8 GHz.

The antennas reported in [14–17] operate on dual frequency bands, with a common operating frequency of 3.5 GHz (3.4–3.6 GHz). The other frequency bands are 5.0 GHz (4.8–5.1 GHz), 5.8 GHz (5725–5875 MHz), and 5.537 GHz (5150–5925 MHz), respectively. The reported antenna unit designs include a foldable monopole linked to a loop branch by a gap, a dual inverted-F/loop structure, fork-like electric dipoles, and stepped impedance resonator-based L-structured slot antennas. Additionally, a dual-mode inverted-F antenna (IFA) has been reported in [18], featuring etched radiators on both the inner and outer sides of the side-part frame. The operating frequencies for this IFA are 3.6/4.9 GHz (3.3–3.6/4.8–5.0 GHz). In [19], the dual-band operating frequencies are 3.6 GHz (3.4–3.8 GHz) and 5.537 GHz (5150–5925 MHz) obtained with a T-shaped coupled-fed slot antenna unit structure.

Among all the articles reported in [4–19], only [13] and [19] operate at a frequency of 3.6 GHz (3.4–3.8 GHz). Most others feature complex antenna element structures that can be exceedingly difficult and costly to fabricate. Therefore, it remains a challenging task for antenna researchers to design simpler antenna structures in the desired band (3.4–3.8 GHz) with improved MIMO performances. Since slot antennas have a simple structure and offer advantages such as good isolation, excellent S-parameters, wide impedance bandwidth, and improved efficiency, these features make them suitable for various applications.

Furthermore a small-sized MIMO antenna with orthogonally positioned elements [20] is proposed that covers the 3.1–11 GHz frequency band. In order to achieve a high bandwidth of 9 GHz (3–12 GHz) with good isolation complicated fractal shape is presented in [21]. In [22], a MIMO antenna operating at ultra-wideband region 3–13.5 GHz with a simple geometry consisting of a partial defected ground structure is presented.

In this article, we develop a MIMO antenna with a simple structure where the fundamental building element is a line slot inside a rectangular patch. The antenna unit measures 28.4 mm $\times$ 6 mm. An aperture coupled feeding mechanism is applied in this article. Due to the asymmetrical feed position or feed point in the proposed antenna element, it provides dual-frequency bands: LB and UB, corresponding to the long-term evolution (LTE) bands 42/43 (i.e., 3.4–3.8 GHz) and 10.5–14.0 GHz, respectively. The performance attributes of the developed MIMO are analyzed in terms of reflection coefficient, isolation, total efficiency, ECC, TARC, MEG, CCL, and CC.

In the LB, measured values for S-parameter, total efficiency, ECC, TARC, $|\text{MEG}_i - \text{MEG}_j|$, CCL, and CC are better than -6 dB, 10 dB, 56%, 0.15, -11 dB, 0.83 dB, and 0.275 bps/Hz, respectively. However, in the UB, values are better than or nearly equal to -6 dB, 10 dB, 40%, 0.2, -5 dB, 1.6 dB, 0.55 bps/Hz, and 33.6 bps/Hz, respectively. The LB is suitable for 5G mobile applications, while the UB can be used for satellite communications. The frequency bands 11.7–12.2 GHz and 12.2–12.7 GHz (covered by the UB) are downlink frequency bands for direct broadcast services (DBSs) and fixed satellite services (FSSs), respectively, as assigned by the International Telecommunication Union (ITU) in region 3. All simulation results are obtained from CST Microwave Studio, and MIMO system is fabricated on an FR4 substrate with 0.8 mm thickness.

2. PROPOSED 8-ELEMENT MIMO ANTENNA SYSTEM

The investigated 8-element MIMO antenna system consists of (i) a system substrate with dimension of 150 mm $\times$ 70 mm and (ii) two small substrates having dimension 150 mm $\times$ 6 mm are vertically fixed along the long edges of the system substrate. Due to the increasing popularity of slim handsets in the present era, the choice of substrate thickness is equally important. In this case, it is 0.8 mm. Figs. 1(a) and 1(b) depict the perspective and side views of the developed MIMO, respectively. Ant1, Ant4, Ant5, and Ant8 are placed near the corner of small substrates which are referred to as Array A elements, whereas Ant2, Ant3, Ant6, and Ant7 are placed amid the short edges of small substrates which are referred to as Array elements. Due to the symmetrical placement of antenna elements (elements of Array A or elements of Array), it provides a low ECCs, satisfactory isolation, good total efficiency, and satisfactory radiation pattern. The adjacent antenna unit distance is either 12.5 mm or 12.6 mm. A 50-ohm feed line is applied to the top of the system substrate, which perpendicularly connects the antenna unit on the feed point.

The feed point is defined as the mid-point of a 50-ohm microstrip line on a small substrate where antenna unit is present. For optimal results in all respects, the feed points on the first small substrate are maintained at 17.7 mm, 58 mm, 92.3 mm and 132.3 mm for elements Ant4, Ant3, Ant2, and Ant1, respectively from edge (CD). In the same manner, the feed points on the second small substrate are maintained at 17.7 mm, 58 mm, 92 mm, and 132.3 mm for elements Ant8, Ant7, Ant6, and Ant5, respectively from edge (AB).

2.1. ANTENNA ELEMENT

Figure 2(a) shows the evolution steps of single antenna element. In step-A, central feeding mechanism is applied on rectangular type patch situated on outer side substrate, which provides dual -6 dB impedance bandwidths which are 8.7–10 GHz and 14.0–15.0 GHz. In second step-B, a line slot is cut from the rectangular patch which provides the triple -6 dB impedance bandwidths which are 8.7–9.9 GHz, 11–12.6 GHz, and 14–15 GHz. Finally, the feed position is maintained at a distance of 3.5 mm from its central position that provides -6 dB dual wider bandwidths which are 3.4–3.8 GHz, applicable to 5G LTE 42/43

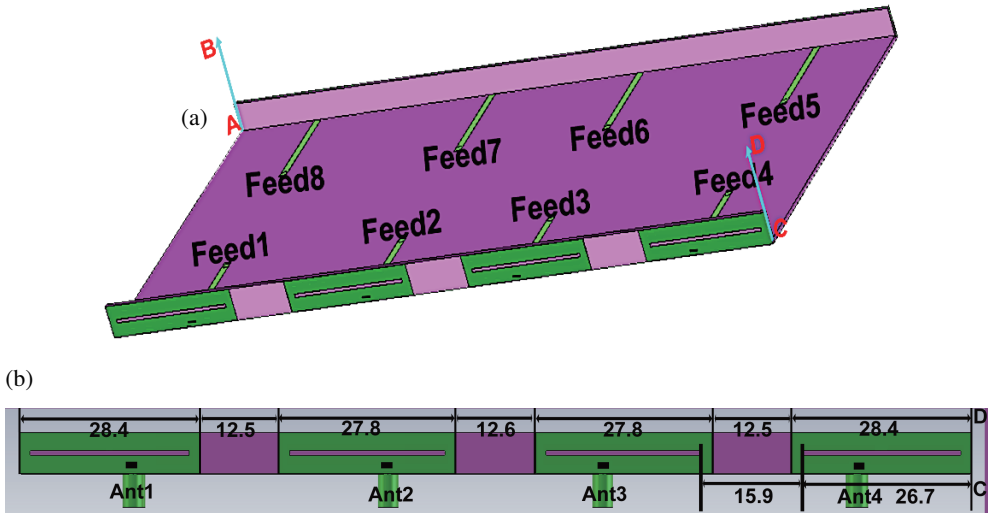

FIGURE 1. Proposed MIMO antenna system, (a) prospective view, (b) side view.

TABLE 1. Values of design variables of antenna elements for optimal performance of developed MIMO system.

Design Variable	Array_A (Ant1, Ant4, Ant5 & Ant8)	Array_B (Ant3, Ant6 & Ant7)	Array_B (Ant2)
Patch_len	28.4 mm	27.8 mm	27.8 mm
Slot_len	25 mm	24.4 mm	24.4 mm
Slot_wid	0.6 mm	0.6 mm	0.6 mm
Feed_pos	3.5 mm	3.2 mm	2.9 mm

band and 10.5–14 GHz. The sizes of the antenna units in Array A and Array are different. The antenna element of Array A has a size of 28.4 mm × 6 mm; however, Array have a size of 27.8 mm × 6 mm. For the optimal result, the line slot lengths of antenna elements of Array A and Array are 25 mm and 24.4 mm, respectively. The constructed antenna unit is shown in Fig. 2(a) with following design variables "*patch_len*", "*slot_len*", "*slot_wid*", and "*feed_len*". "*patch_len*" indicates the total length of the rectangular patch; "*slot_len*" means the total length of the line slot; "*slot_wid*" indicates the width of the line slot; and "*feed_pos*" implies the distance of feed point position from the midpoint of the antenna element in the same level. For the optimum execution of the MIMO antenna system, the design variables of elements of Array A and Array are introduced in Table 1.

Figure 2(b) shows the constructed antenna unit's corresponding lumped circuit model, which consists of a parallel connection of two LC series circuits, series connection of two LCR parallel circuits, and a resistor, and all are connected in series with port and ground. For the optimal result following lumped component values are taken which are $C1 = 0.1\,\mu$F, $C2 = 1\,\mu$F, $C3 = 2\,\mu$F, $C4 = 0.1\,\mu$F, $L1 = 1.7$ nH, $L2 = 2$ nH, $L3 = 1.6$ nH, $L4 = 0.1$, $L5 = 0.1$ nH, $L6 = 0.1$ nH, $R1 = 57$ Ohm, $R2 = 47$ Ohm, and $R3 = 30$ Ohm.

Figure 3 illustrates the interfacial current patterns at the frequencies of 3.54 GHz, 10.9 GHz, and 13.9 GHz. Here, it is evident in Fig. 3(a) that a strong interfacial current concentrates around the slot in two equal parts with one null space width (W_{ns}) between them. It is clear in Fig. 3(b) that a strong interfacial current concentrates around the slot in four equal parts with three equal null space widths ($\frac{W_{ns}}{3}$) between them. Similarly, Fig. 3(c) indicates that a strong interfacial current concentrates around the slot in five equal parts with four equal null space widths ($\frac{W_{ns}}{4}$) between them.

Here, the length of radiating patch would be equal to half of the medium's wavelength at the resonance, and this can be calculated using following equations

$$L_{3.54} = \frac{2 * slot_{len}}{2} - 2W_{ns} \tag{1}$$

$$L_{10.9} = \frac{2 * slot_{len}}{6} - \frac{2W_{ns}}{3} \tag{2}$$

$$L_{13.9} = \frac{2 * slot_{len}}{8} - \frac{2W_{ns}}{4} \tag{3}$$

where $L_{3.54}$, $L_{10.9}$, and $L_{13.9}$ are the radiating patch lengths for the resonance frequencies 3.54 GHz, 10.9 GHz, and 13.9 GHz, respectively.

Equation (4) can be used to calculate resonance frequency (f_r).

$$f_r = \frac{c}{2L\sqrt{\epsilon}_{reff}} \tag{4}$$

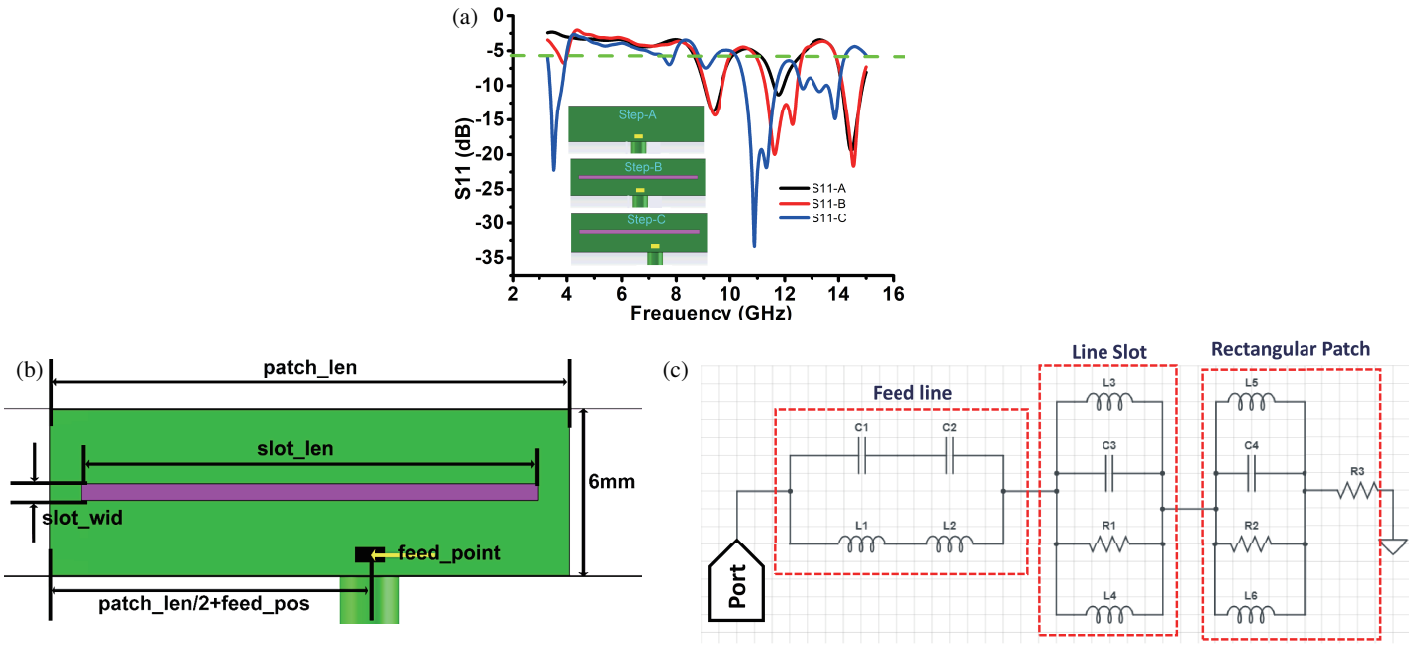

FIGURE 2. (a) Evolution of sigle antyenna unit. (b) Developed structure of antenna unit. (c) Lumped circuit model of antenna unit.

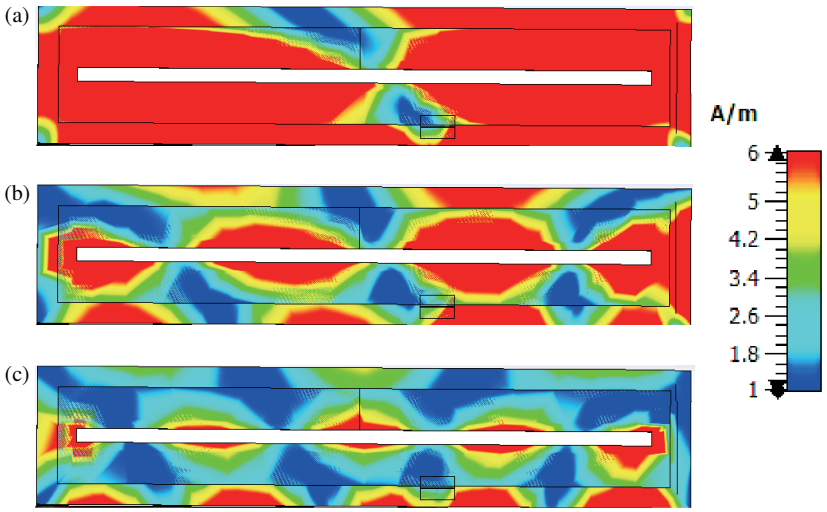

FIGURE 3. Simulated interfacial current patterns at (a) 3.54 GHz, (b) 10.9 GHz and (c) 13.9 GHz.

where L is the lengths of radiating patch (i.e., $L_{3.54}$, $L_{10.9}$, and $L_{13.9}$), and $\in_{reff}$ is the effective dielectric constant which can be calculated using Equation (5)

$$\text{For } \frac{W_f}{h} \geq 1,\ \epsilon_{reff} = \frac{\epsilon_r+1}{2} + \frac{\epsilon_r-1}{2}\left\{\left(1+12\frac{h}{W_f}\right)^{-0.5}\right\} \quad (5)$$

where h is the thickness of substrate, and W_f is the width of microstrip feed line. In this article, $h = 0.8$ mm, $\epsilon_r = 4.4$, and $W_{ns} = W_f = 1.5$ mm.

From the above equations, the effective dielectric constant, radiating patch lengths, and resonant frequencies are calculated which are listed in Table 2.

2.2. Parametric Investigation of Developed Antenna Unit

In this section, the reflection coefficient ($\mathbf{S_{11}}$) is investigated by changing any one of the design variables and preserving other variables to optimum level. For this investigation, Ant1 of Array_A is chosen. When the design parameter "feed$_{pos}$" is varied from its optimal value conditionally (i.e., keeping all other design parameters optimally constant), it is observed that decreasing the value of "feed$_{pos}$" results in a decrease in $\mathbf{S_{11}}$ at resonance and -6 dB impedance bandwidth; however, increasing the value of "feed$_{pos}$" results in a shift in -6 dB impedance bandwidth towards the higher frequency side, as illustrated in Fig. 4(a). Moving to the next design parameter "patch$_{len}$": when it increases from its optimum value, the -6 dB impedance

TABLE 2. Calculated resonance frequencies and % difference.

Parameters	Calculated Values	Resonant Frequency (f_r)		% difference of f_r
		Simulated value (GHz)	Calculated value (GHz)	
$\in_{reff}$	3.051			
$L_{3.54}$	25.4 mm	3.54	3.38	4.52
$L_{10.9}$	8.467 mm	10.9	10.14	6.98
$L_{13.9}$	6.35 mm	13.9	13.52	2.73

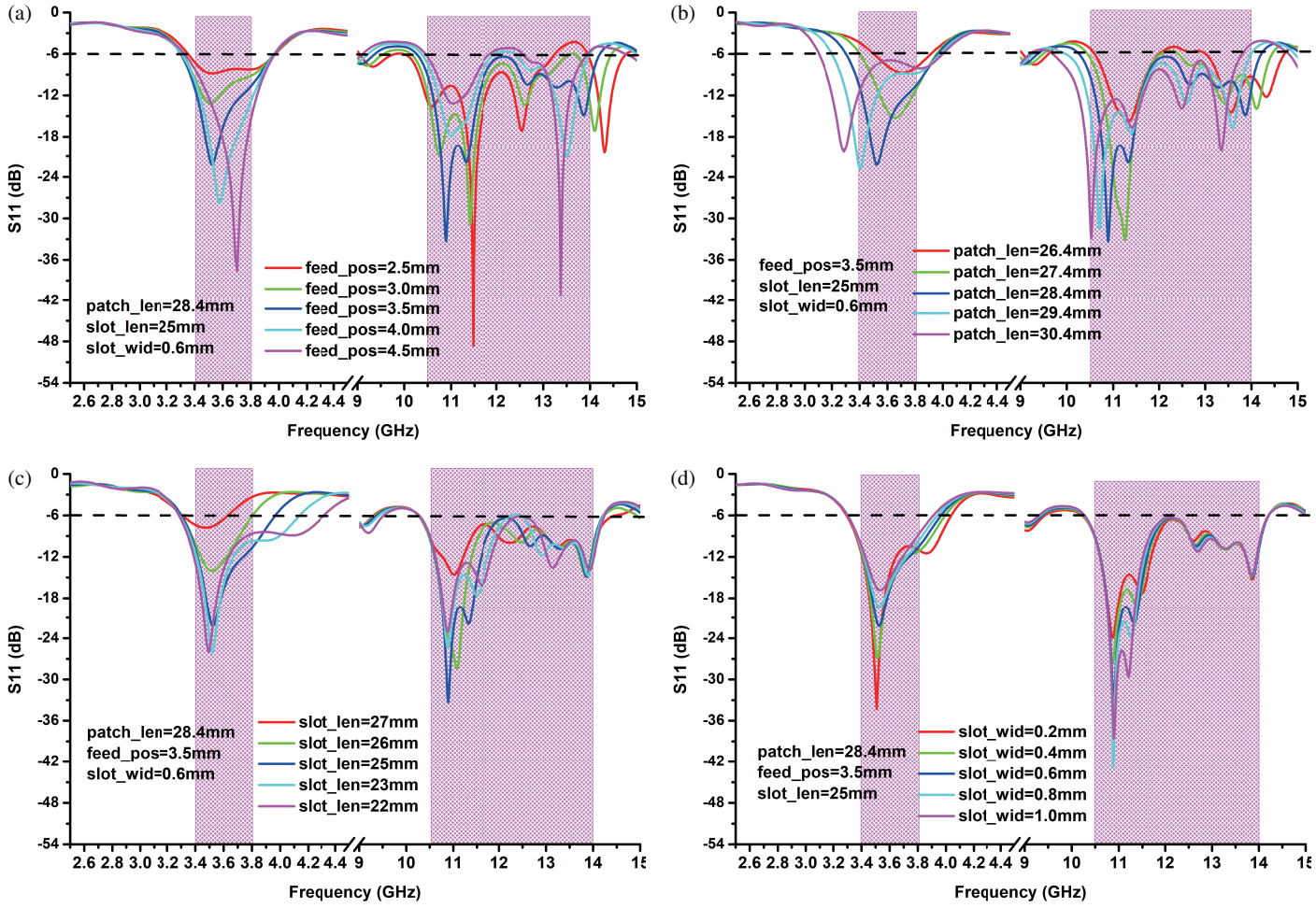

FIGURE 4. $\mathbf{S_{11}}$ outcomes for distinct magnitude of (a) feed_pos, (b) patch_len, (c) slot_len and (d) slot_wid.

bandwidth shifts towards the lower side; however, decreasing the parameter value results in a higher value of -6 dB impedance bandwidth which is illustrated in Fig. 4(b). As shown in Fig. 4(c), it is confirmed that when the design parameter "slot$_{len}$" varies (increasing or decreasing) from its optimum value, this decreases $\mathbf{S_{11}}$ at resonance. Lastly, it is observed that decreasing the value of the design parameter "slot$_{wid}$" results in the higher -6 dB impedance bandwidth; however, increasing the value of the parameter provides the lower bandwidth which is depicted in Fig. 4(d).

3. PERFORMANCE OF DEVELOPED MIMO ANTENNA

Performance analysis of the constructed 8-port MIMO antenna is presented in this section. The section goes into detail on S-parameters, Radiation Pattern, Total Antenna Efficiency, Mean Effective Gain, Channel Capacity Loss, Total Active Reflection Coefficient, and Envelope Correlation Coefficient. The perspective view of the manufactured MIMO is displayed in Fig. 5(a). The performance of suggested MIMO antenna was evaluated with the restriction that, when the exciting unit was being measured, the other elements should be ended to match loads. Vector network analyzer (VNA) is used to evaluate S-

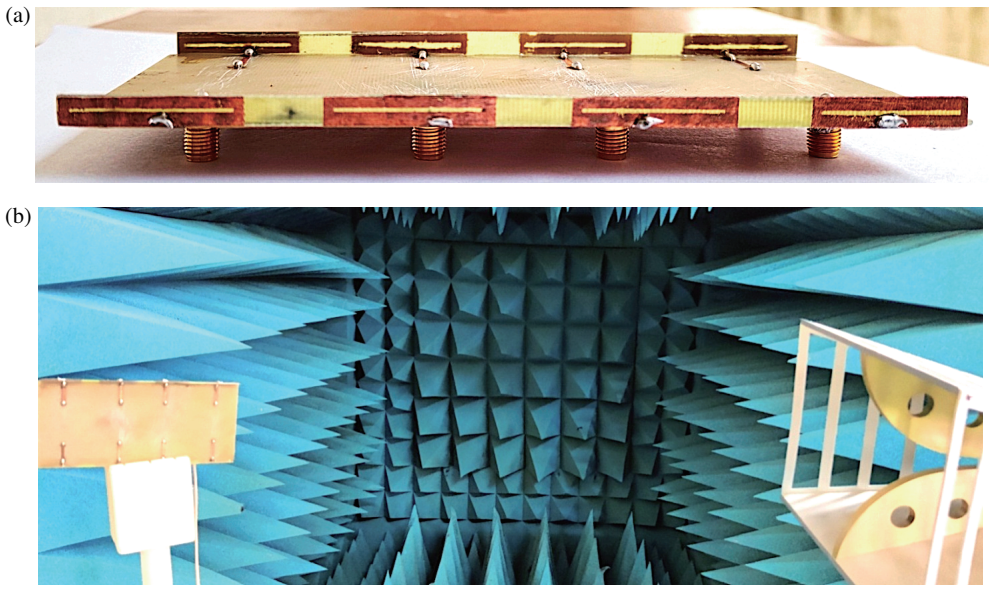

FIGURE 5. Images of (a) developed 8x8 MIMO antenna. (b) Setups for measuring radiation characteristics and efficiency.

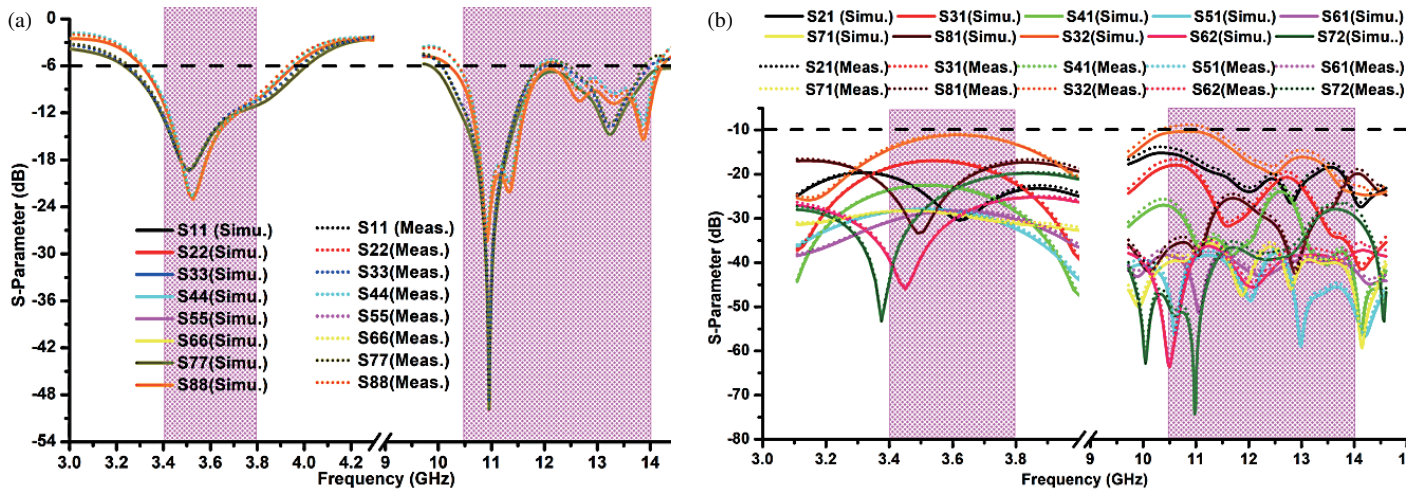

FIGURE 6. Simulated and measured value of (a) reflection coefficient (b) port isolation.

parameters. Fig. 5(b) depicts the anechoic chamber for the measurement of radiation patterns and antenna efficiency.

The measured values are compared with simulation one, and a good concurrence between simulation and measurement is achieved. Some minor variations are due to the fabrication imperfection and soldering standard of SMA connectors. The reflection coefficient (S_{mm}, where $1 \leq m \leq 8$) of all antennas is depicted in Fig. 6(a). Over the LB and UB the simulated and measured values of reflection coefficient are better than or nearly equal to -6 dB. The simulated and measured values of isolation between ports (S_{mn}, where $m \neq n$ and $1 \leq n \leq 8$), are depicted in Fig. 6(b). In the entire band of LB, the measured value is better than -10.3 dB, however in UB the measured value less than -10 dB.

The simulated & measured 2D radiation patterns of Array_A and Array_B elements are illustrated in Fig. 7 and Fig. 8, respectively. The 2D radiation patterns of all antenna elements are analyzed in XZ, YZ, and XY planes at the frequency of 3.6 GHz. The copolar or the crosspolar radiation patterns in planes XZ, YZ, and XY of Array_A elements (i.e., Ant1, Ant4, Ant5, and Ant8) are either complement or perpendicular to one another in the same plane. In the same fashion, the copolar or crosspolar radiation patterns in planes XZ, YZ, and XY of Array_B elements (i.e., Ant2, Ant3, Ant6, and Ant7) are either complement or perpendicular to one another in the same plane.

From Fig. 7 and Fig. 8, it is investigated that the simulated and measured co-polarization radiation patterns of any of the antenna units of Array_A or Array_B in comparison to other antenna units (situated in the same Array) in planes XZ, YZ, and XY are either complement or perpendicular; furthermore, the cross-polarization radiation patterns are nearly complement or orthogonal.

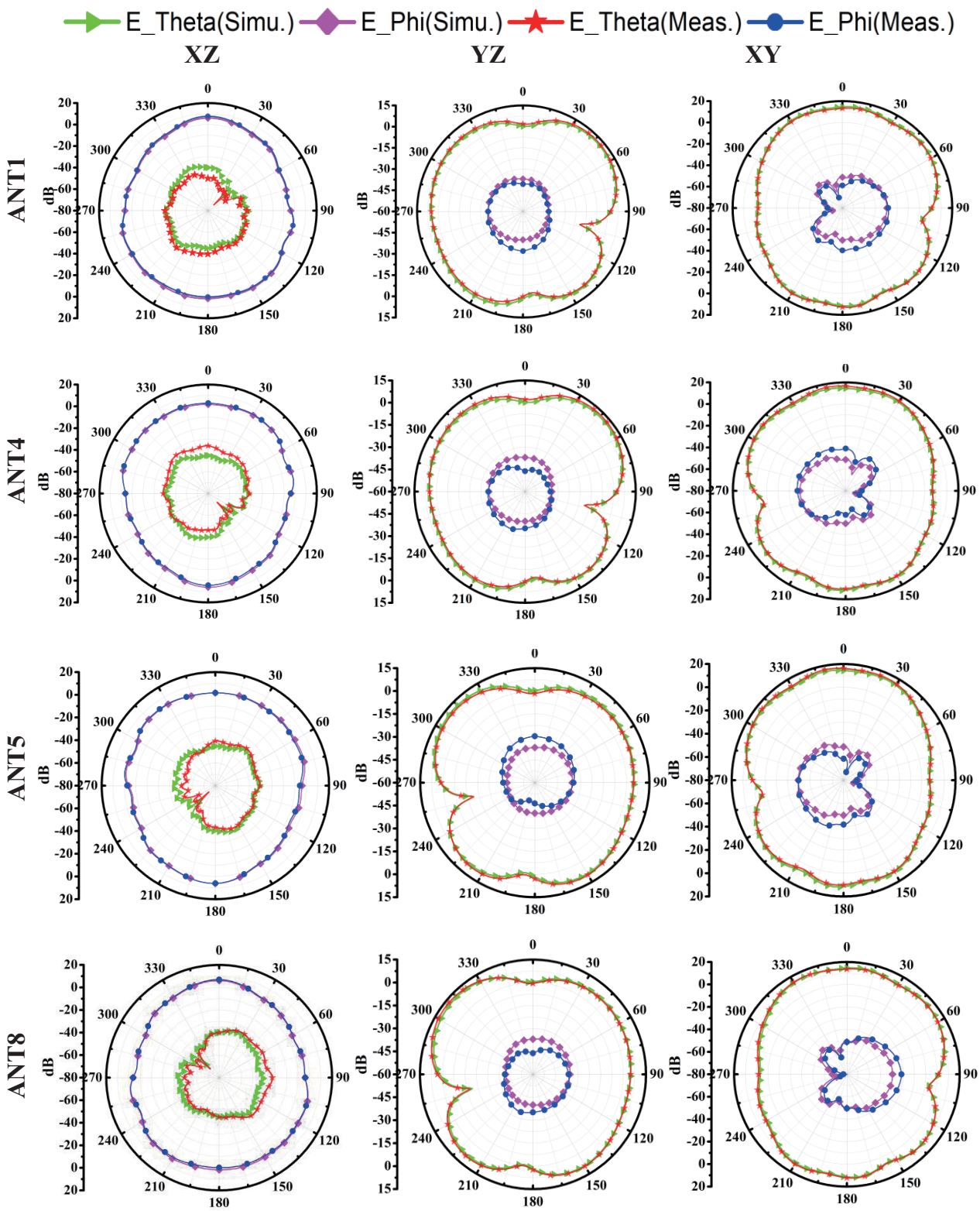

FIGURE 7. Simulated & Measured Radiation pattern of Array_A elements in XY, YZ and XZ plane @3.6 GHz.

As explained in [23], antenna components arranged in a symmetrical manner as well as the similarity, complementary, and orthogonality characteristics of radiation patterns are advantageous for achieving smaller ECCs in both frequency LB and UB.

The antenna elements of Array_A are placed symmetric to one another which promotes the nearly equal total efficiency in LB and UB. Furthermore, the same is happening in Array_B, which also promotes the nearly equal total efficiency in LB and UB for each antenna element of Array_B.

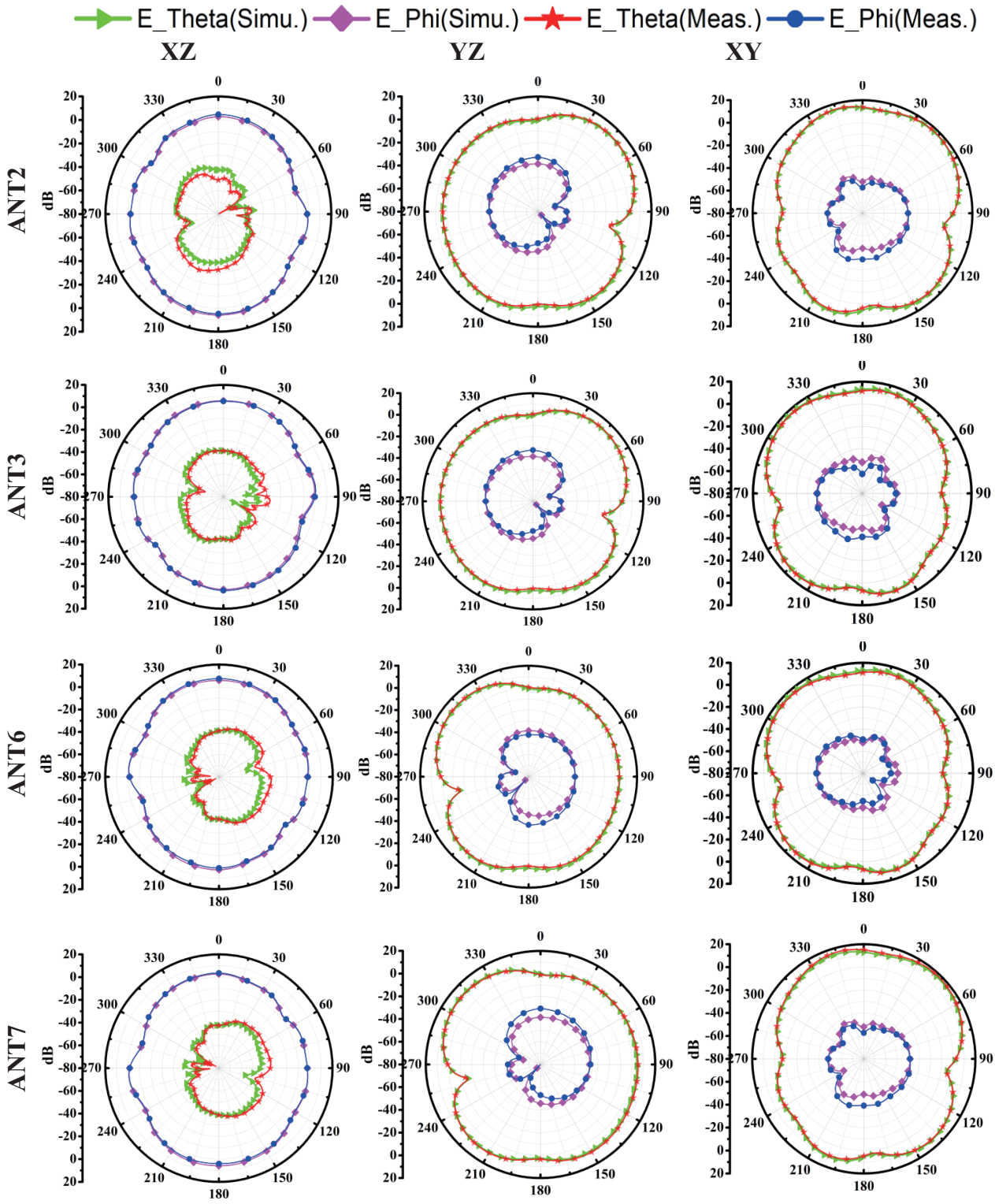

FIGURE 8. Simulated & Measured Radiation pattern of Array_B elements in XY, YZ and XZ plane @3.6 GHz.

Due to this reason, simulated and measured results for the total efficiency of Ant1 of Array_A and Ant2 of Array_B are identified. The simulated results of total efficiency within LB of Array_A and Array_B elements are 63.1–73.6% and 61–64.2%, respectively, whereas the measured results are 58–70.1% and 56.2–61.5%, respectively. The simulation results of total efficiency within UB of Array_A and Array_B elements are $41 \sim 60\%$ and $46 \sim 57\%$, respectively, whereas the measured results are 40.2–57.3% and 43.3–51.3%, respectively.

The simulated and measured results of total efficiency for Array_A and Array_B are evidenced in Fig. 9(a). The suit-

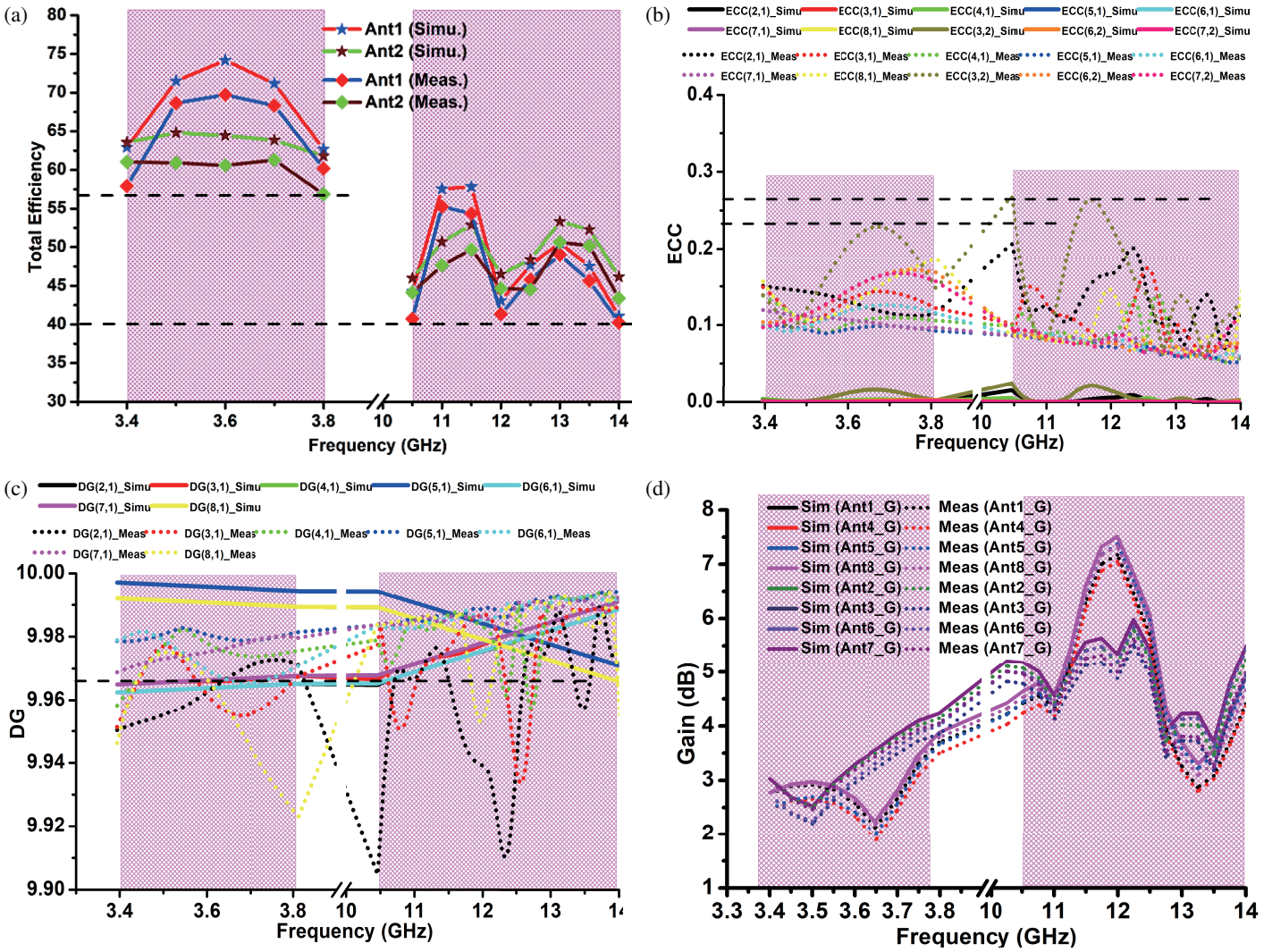

FIGURE 9. The simulated and measured value of (a) total efficiency (b) ECC (c) DG (d) Gain.

ability of MIMO antenna (in LB and UB) can be checked by various diversity characteristics parameters. One of them is envelope correlation coefficient (ECC). The MIMO antenna system's outstanding diversity gain and high isolation are indicated by the ECC values that are closest to zero. The simulation and measurement values of ECC are depicted in Fig. 9(b).

The ECC value in the case of simulation is better than 0.02 over the entire range of LB and UB; however, the measurement value of ECC is better than 0.15 and 0.2 in LB and UB, respectively. The measured ECC is computed by Equation (6) [24].

$$\mathrm{ECC} = \rho_{i,j} = \frac{\left|\iint_{4\pi}\left[\vec{M}_i(\theta,\varphi)\cdot\vec{M}_j(\theta,\varphi)\right]d\Omega\right|^2}{\left[\iint_{4\pi}\left|\vec{M}_i(\theta,\varphi)\right|^2 d\Omega\right]\cdot\left[\iint_{4\pi}\left|\vec{M}_j(\theta,\varphi)\right|^2 d\Omega\right]} \quad (6)$$

where $\vec{M}_i(\theta,\varphi)$ describes the 3D radiation pattern when antenna 'i' is excited, and $\vec{M}_j(\theta,\varphi)$ describes the 3D radiation pattern when antenna 'j' is excited. The solid angle in the above Equation (6) is represented as Ω.

The measured value of ECC is better than 0.23 over the LB and 0.26 over the UB, which is lower than the acceptable value of 0.5, and this promise a good candidature to use the MIMO antenna for 5G and satellite applications.

Diversity gain (DG) is defined as the amount of advancement gained by an array system in comparison to a single element and is calculated by equation (7)

$$\mathrm{DG} = 10\sqrt{1-\mathrm{ECC}^2} \quad (7)$$

DG should be approximately 10 dB. The measured value of DG in LB is 9.92 dB, however in UB is 9.91 dB which is shown in Fig. 9(c).

The port gain of all ports of fabricated MIMO system is measured. In LB the maximum gain is 4.1 dB; however in UB the maximum port gain is 7.2 dB which is depicted in Fig. 9(d).

Another valuable diversity characteristics parameter of MIMO system is mean effective gain (MEG). It differentiates the radiation gained by the diversity antenna to the isotropic antenna in a fading scenario.

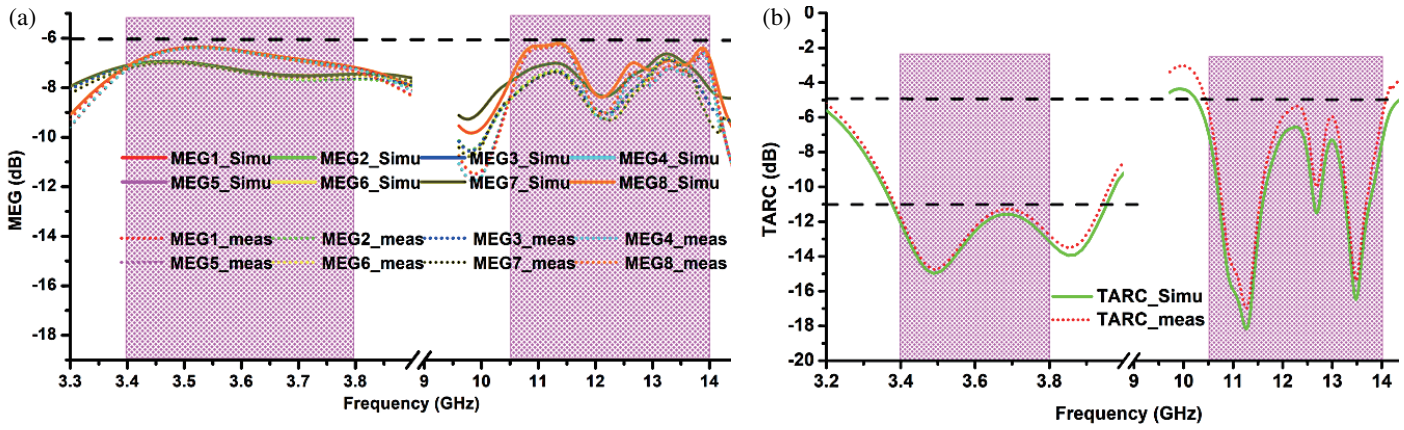

FIGURE 10. Simulated and measured. (a) MEG (b) TARC.

The MEG of the ith antenna is determined by Equation (8) [25].

$$\mathrm{MEG}_i = 0.5\left[1 - \sum_{n=1}^{N} |S_{in}|^2\right] \tag{8}$$

The simulated and measured values of MEG_i over LB and UB are illustrated in Fig. 10(a). The MIMO performance can be observed by evaluating the value of $|\mathrm{MEG}_i - \mathrm{MEG}_j|$ for all possible values of i and j where $i \neq j$, and i, j vary from 1 to 8.

It is noted that over the LB the maximum simulated and measured values of $|\mathrm{MEG}_i - \mathrm{MEG}_j|$ are 0.78 dB and 0.83 dB respectively at frequency 3.6 GHz; however, the maximum simulated and measured values over UB are 1.36 dB and 1.6 dB respectively at the frequency 13.93 GHz.

For 5G and satellite operation, the standard value of $|\mathrm{MEG}_i - \mathrm{MEG}_j|$ is lower than 3 dB. Here, the measured $|\mathrm{MEG}_i - \mathrm{MEG}_j|$ is 1.6 dB over both LB and UB which are nicely sufficient for 5G and satellite operations.

The next diversity characteristics parameter of the MIMO system is the total active reflection coefficient (TARC). It is calculated by dividing the square root of the overall incident power by the square root of the overall reflected power[29]. Because TARC takes into account information regarding the mutual coupling effect, it offers a valuable way to measure MIMO antenna efficiency. For an N-element MIMO antenna system, TARC equation can be calculated using Equation (9) [27].

$$\mathrm{TARC} = N^{-0.5}\sqrt{\sum_{i=1}^{N}\left|\sum_{K=1}^{N} S_{ik}e^{j\theta_{k-1}}\right|^2} \tag{9}$$

Equation (9) is used to calculate TARC on the premise that $\theta_i = 0$ (where $i = 1$ to $N - 1$ and $N = 8$). Fig. 10(b) displays the simulated and measured TARCs. Over LB and UB the simulated and measured values of TARC are less than -11 dB and -5 dB, which are sufficient enough for 5G and satellite operation.

Another crucial diversity characteristics parameter inspection for MIMO antennas is channel capacity loss (CCL). It explains the fastest possible rate at which data can be sent, without suffering significant losses. The CCL can be calculated using Equation (10) [28].

$$\mathrm{CCL} = -\log_2\left[\det\left(\varphi^R\right)\right] \tag{10}$$

where

$$\varphi^R = \begin{pmatrix} \alpha 11 & \alpha 12 & . & . & \alpha 1N \\ \alpha 21 & \alpha 22 & . & . & \alpha 2N \\ . & . & . & . & . \\ . & . & . & . & . \\ \alpha N1 & \alpha N2 & . & . & \alpha NN \end{pmatrix},$$

$$\left(\alpha ii = 1 - \left(\left|\sum_{j=1}^{j=N} S_{ij}^* S_{ji}\right|\right)\right),$$

$$\left(\alpha ik = -\left|\sum_{j=1}^{j=N} S_{ij}^* S_{jk}\right|\right),$$

$1 \leq i \leq N,\ 1 \leq k \leq N$ and $N = 8$

Figure 11(a) shows the simulated and measured CCLs for LB and UB. The highest simulated and measured values of CCL over LB are 0.25 bps/Hz and 0.28 bps/Hz, respectively; however, the maximum simulated and measured values of CCL over UB are 0.4 bps/Hz and 0.55 bps/Hz, respectively. For the 5G and satellite operation, the CCL should be less than or equal to 0.5 bps/Hz. In this article, it is 0.275 bps/Hz over LB and approximately 0.5 bps/Hz over UB, which are sufficient for a 5G and satellite operation.

The ergodic Channel Capacity is another important metric that provides information on the diversity characteristics of a MIMO system, and it is computed under the assumption that there are no ECCs between the transmitting antennas.

Equation (11) is used to compute the ergodic MIMO channel capacity (CC) [30].

$$C = E\left\{\log_2\left[\det\left(I + \frac{\mathrm{SNR}}{n_T}HH^H\right)\right]\right\} \tag{11}$$

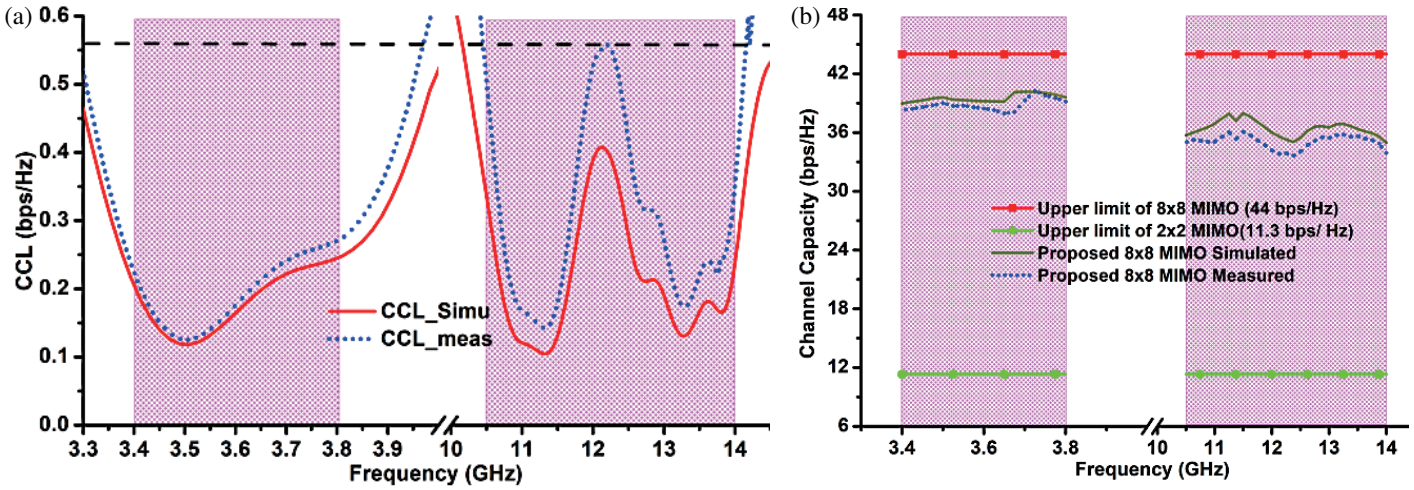

FIGURE 11. Simulated & measured value of (a) CCL (b) CC.

TABLE 3. Comparison between the proposed design and the referenced antennas for 5G mobile applications.

Ref. No	System Substrate Dimension mm^3	MIMO Order	Frequency band in GHz (-10 dB Impedance Bandwidth)	Isolation (dB)	ECC	Range of antenna efficiency (%)	MEGi-MEGj (dB)	TARC (dB)	CCL (bps/Hz)	CC (bps/Hz)
[4]	$136 \times 68 \times 1$	8	2.55–2.65	> 12	< 0.15	48–55	< 1	-	-	38–40
[5]	$136 \times 68 \times 6$	8	2.55–2.65	> 13	< 0.2	48–57	< 1			37–39
[6]	$150 \times 75 \times 0.8$	8	3.4–3.6 (SDIB)	> 17	< 0.07	49–56.4	-	-	-	-
[7]	$150 \times 75 \times 0.8$	8	3.4–3.6 (SDIB)	> 14	< 0.15	$40 \sim 52$	< 1.5	-	-	~ 35
[8]	$150 \times 75 \times 0.8$	8	3.4-3.6	> 20	< 0.03	> 60	-	-	-	> 35
[9]	$150 \times 75 \times 0.8$	8	3.4–3.6	> 19.6	< 0.0125	> 60	-	-	-	> 34
[10]	$136 \times 68 \times 1.6$	6	3.4–3.6	≥ 30	< 0.15	50–60	≥ 0.3	-	-	31.2(PCC)
[11]	$140 \times 75 \times 0.8$	10	3.4–3.6	> 11	< 0.15	50–76	-	-	-	48–51
[12]	$136 \times 68 \times 0.8$	8	3.3–3.7 (SDIB)	> 15	< 0.1	50–75	0.3	-	-	38.1(PCC)
[13]	$140 \times 70 \times 0.8$	10	3.4–3.8 (SDIB)	> 10	< 0.1	38–62	-	-	-	43–47
[14]	150 x 75 x 0.8	8	3.4–3.6 (SDIB)	> 11.5	< 0.08	41-72	< 1.6	-	-	37–38.5
			4.8–5.1 (SDIB)	> 11.5	< 0.05	40–85	< 1.6	-	-	37–38.5
[15]	150 x 74 x 0.8	8	3.4–3.6 (SDIB)	> 12	< 0.15	~ 55	-	-	-	~ 37
			5.725–5.875 (SDIB)	> 12	< 0.15	~ 70	-	-	-	~ 42
[17]	$140 \times 70 \times 1$	8	3.4-3.6	> 11.2	< 0.08	51- 59	-	-	-	36.9–37.9
			5.15–5.925	> 11.2	< 0.08	62-80	-	-	-	38.5–40.9
[18]	$150 \times 70 \times 0.8$	10	3.4–3.6 (SDIB)	> 12	< 0.15	45–78	-	-	-	46-51
			4.8-5.0 (SDIB)	> 12	< 0.15	45–65	-	-	-	46–51
[19]	150 x 80 x 0.8	10	3.4–3.8 (SDIB)	> 11	< 0.15	42–65	< 1 (MEGR)	-	-	45–48
			5.15–5.925 (SDIB)	> 11	< 0.05	62–82	< 1 (MEGR)	-	-	50–51.4
Proposed	$\mathbf{150 \times 70 \times 0.8}$	**8**	**3.4–3.8 (SDIB)**	$\mathbf{> 10}$	$\mathbf{< 0.15}$	**56–61**	$\mathbf{\geq 0.831}$	$\mathbf{< -11}$	$\mathbf{\leq 0.275}$	$\mathbf{38 \sim 40.2}$

*SDBI $\rightarrow$ At -6 dB impedance bandwidth, *MEGR $\rightarrow \left(\frac{\text{MEG}_i}{\text{MEG}_j}\right)$, *PCC $\rightarrow$ Peak channel capacity, *SR $\rightarrow$ Simulated result

where n_T is the number of transmitting antennas; E stands for the expectation with regard to various channel realizations; SNR is the mean signal to noise ratio at the receiving side; H^H stands for the Hermitian transpose; and I is an identity matrix.

Our analysis of over 10,000 Rayleigh fading realizations with a 20 dB SNR assumes 100% antenna efficiency and no ECC between antennas to find the optimal CC for N-element MIMO antenna systems. In the case of $N = 2$ and $N = 8$, the optimum CC is calculated which are 11.3 bps/Hz and 44 bps/Hz, respectively. The measured CC of the 8×8 MIMO antenna system is based on the average of more than 10,000 Rayleigh fading realizations with an SNR of 20 dB under the assumption that the

transmitter side has eight separate uncorrelated antennas. The simulated and measured CCs over LB are $39 \sim 40.2$ bps/Hz and $38 \sim 40.2$ bps/Hz, respectively, and CCs over UB are $35 \sim 38$ bps/Hz and $33.6 \sim 36.1$ bps/Hz, respectively.

Figure 11(b) shows the findings of ergodic 8×8 MIMO channel capacity in the target ranges LB and UB. Fig. 11(b) shows that the maximum CC value (over LB and UB) is approximately 3.3 times of the optimal CC value for a 2×2 MIMO antenna system. This confirms that the developed MIMO antenna setup is suitable for 5G and satellite operation.

Furthermore, the comparative study of recently reported MIMO antennas has been done which is elaborated in Table 3. It is observed that the dimension of system substrate of constructed MIMO antenna is smaller than [6–9, 14, 15, 19]; however it is bigger than [4, 5, 10–13, 17, 18]. The coverage of LB is only reported in [13, 19], and none of the articles reports the UB. The suggested MIMO antenna has a higher antenna efficiency over the LB bandwidth than [4–7, 11, 17]. $|\text{MEG}_i - \text{MEG}_j|$ plays a significant role in understanding the diversity performance of the MIMO system; however, many of recently reported articles did not make the calculation which are [6, 8, 9, 11, 13, 15–18]. There are no measurements of TARC and CCL (overall MIMO) for recently reported referenced antennas. A key component of evaluating MIMO diversity performance is to measure the TARC and CCL. These values should be $(0 \leq \text{TARC} < 1)$ and $(0\frac{\text{bps}}{\text{Hz}} < \text{CCL} \leq 0.5\frac{\text{bps}}{\text{Hz}})$, respectively. The highest TARC and CCL in the present study over LB are 0.0745 (i.e., -11.28 dB) and 0.275 bps/Hz, respectively. Finally, using Table 2, a comparative analysis of CC is conducted, and it was noted that the planned MIMO antenna system's CC outperforms LB values of [4, 5, 7–9, 12, 14].

4. CONCLUSION

A dual-band (3.4–13.8 GHz and 10.5–14.0 GHz) eight-port multiple-input multiple-output (MIMO) antenna is developed in this article. A line slot inside a rectangular patch serves as the fundamental construction unit of antenna element. The diversity attributes of the developed MIMO antenna are inspected in terms of the reflection coefficient, port isolation, total efficiency, ECC, TARC, $|\text{MEG}_i - \text{MEG}_j|$, CCL, and CC. In LB, the measured values of reflection coefficient, isolation between the ports, total efficiency, ECC, TARC, $|\text{MEG}_i - \text{MEG}_j|$, CCL & CC are respectively better than -6 dB, 10 dB, 56%, 0.15, -11 dB, 0.83 dB, 0.275 bps/Hz, and 38 bps/Hz, respectively; however in UB the measured values are -6 dB, 10 dB, 40%, 0.2, -5 dB, 1.6 dB, 0.4 bps/Hz, and 33.6 bps/Hz, respectively. The practical values of reflection coefficient, isolation between the ports, total efficiency, ECC, TARC, $|\text{MEG}_i - \text{MEG}_j|$, CCL & CC should be ≤ -6 dB, ≤ -10 dB, $\geq 40\%$, ≤ 0.5, ≤ 0 dB, ≤ 3 dB, ≤ 0.5 bps/Hz, and $\geq 60\%$ of upper limit of 8×8 MIMO (i.e., 26.5 bps/Hz). In the LB and UB regions, the proposed MIMO antenna satisfies all of the aforementioned requirements, suggesting that it would be a good fit for 5G mobile and satellite applications (DBS and FSS).

ACKNOWLEDGEMENT

The authors wish to express their profound gratitude to Universiti Teknikal Malaysia Melaka (UTeM) for their generous support. This work was made possible through the grant PJP/2024/FTKEK/PERINTIS/S01388. Their assistance and resources have been instrumental in the successful completion of this research.

REFERENCES

[1] Agiwal, M., A. Roy, and N. Saxena, "Next generation 5G wireless networks: A comprehensive survey," *IEEE Communications Surveys & Tutorials*, Vol. 18, No. 3, 1617–1655, 2016.

[2] Kaur, I., B. Basu, and A. Singh, "Sub-6 GHz metallic via integrated MIMO antenna array for 5G smartphone," *Progress In Electromagnetics Research C*, Vol. 138, 91–104, 2023.

[3] Khade, S. S., D. B. Bhoyar, K. Kotpalliwar, C. V. Bawankar, and M. S. Kimmatkar, "Four element EC slot MIMO antenna for WLAN, Wi-Fi, and 5G applications," *Progress In Electromagnetics Research C*, Vol. 139, 147–158, 2023.

[4] Elabd, R. H. and A. J. A. Al-Gburi, "Ultra-compact 4-port MIMO antenna with defected ground structure and SAR analysis for 28/38 GHz 5G mobile devices," *Journal of Electromagnetic Waves and Applications*, Vol. 38, No. 9, 1–26, 2024.

[5] Li, M.-Y., Z.-Q. Xu, Y.-L. Ban, C.-Y.-D. Sim, and Z.-F. Yu, "Eight-port orthogonally dual-polarised MIMO antennas using loop structures for 5G smartphone," *IET Microwaves, Antennas & Propagation*, Vol. 11, No. 12, 1810–1816, 2017.

[6] Elabd, R. H. and A. J. A. Al-Gburi, "Low mutual coupling miniaturized dual-band quad-port MIMO antenna array using decoupling structure for 5G smartphones," *Discover Applied Sciences*, Vol. 6, No. 4, 189, 2024.

[7] Kumar, P., A. K. Singh, R. Kumar, R. Sinha, S. K. Mahto, A. Choubey, and A. J. A. Al-Gburi, "High isolated defected ground structure based elliptical shape dual element MIMO antenna for S-band applications," *Progress In Electromagnetics Research C*, Vol. 143, 67–74, 2024.

[8] Pandya, K., T. Upadhyaya, U. Patel, V. Sorathiya, A. Pandya, A. J. A. Al-Gburi, and M. M. Ismail, "Performance analysis of quad-port UWB MIMO antenna system for sub-6 GHz 5G, WLAN and X band communications," *Results in Engineering*, Vol. 22, 102318, 2024.

[9] Thakur, E., N. Jaglan, A. Gupta, and A. J. A. Al-Gburi, "Multiband notched circular polarized MIMO antenna for ultrawideband applications," *Progress In Electromagnetics Research M*, Vol. 125, 87–95, 2024.

[10] Ali, A., M. E. Munir, M. M. Nasralla, M. A. Esmail, A. J. A. Al-Gburi, and F. A. Bhatti, "Design process of a compact tri-band MIMO antenna with wideband characteristics for sub-6 GHz, Ku-band, and millimeter-wave applications," *Ain Shams Engineering Journal*, Vol. 15, No. 3, 102579, 2024.

[11] Deng, J.-Y., J. Yao, D.-Q. Sun, and L.-X. Guo, "Ten-element MIMO antenna for 5G terminals," *Microwave and Optical Technology Letters*, Vol. 60, No. 12, 3045–3049, 2018.

[12] Abdullah, M., A. Altaf, M. R. Anjum, Z. A. Arain, A. A. Jamali, M. Alibakhshikenari, F. Falcone, and E. Limiti, "Future smartphone: MIMO antenna system for 5G mobile terminals," *IEEE Access*, Vol. 9, 91 593–91 603, 2021.

[13] Wong, K.-L. and J.-Y. Lu, "3.6-GHz 10-antenna array for MIMO operation in the smartphone," *Microwave and Optical Technology Letters*, Vol. 57, No. 7, 1699–1704, 2015.

[14] Guo, J., L. Cui, C. Li, and B. Sun, "Side-edge frame printed eight-port dual-band antenna array for 5G smartphone applications," *IEEE Transactions on Antennas and Propagation*, Vol. 66, No. 12, 7412–7417, 2018.

[15] Wong, K.-L., B.-W. Lin, and B. W.-Y. Li, "Dual-band dual inverted-f/loop antennas as a compact decoupled building block for forming eight 3.5/5.8-GHz MIMO antennas in the future smartphone," *Microwave and Optical Technology Letters*, Vol. 59, No. 11, 2715–2721, 2017.

[16] Li, Y., H. Zou, M. Wang, M. Peng, and G. Yang, "Eight-element MIMO antenna array for 5G/sub-6 GHz indoor micro wireless access points," in *2018 International Workshop on Antenna Technology (IWAT)*, 1–4, Nanjing, China, 2018.

[17] Li, J., X. Zhang, Z. Wang, X. Chen, J. Chen, Y. Li, and A. Zhang, "Dual-band eight-antenna array design for MIMO applications in 5G mobile terminals," *IEEE Access*, Vol. 7, 71 636–71 644, 2019.

[18] Hu, W., X. Liu, S. Gao, L.-H. Wen, L. Qian, T. Feng, R. Xu, P. Fei, and Y. Liu, "Dual-band ten-element MIMO array based on dual-mode IFAS for 5G terminal applications," *IEEE Access*, Vol. 7, 178 476–178 485, 2019.

[19] Li, Y., Y. Luo, G. Yang, *et al.*, "Multiband 10-antenna array for sub-6 GHz MIMO applications in 5-G smartphones," *IEEE Access*, Vol. 6, 28 041–28 053, 2018.

[20] Anitha, R., P. V. Vinesh, K. C. Prakash, P. Mohanan, and K. Vasudevan, "A compact quad element slotted ground wideband antenna for MIMO applications," *IEEE Transactions on Antennas and Propagation*, Vol. 64, No. 10, 4550–4553, 2016.

[21] Ali, W. A. E. and A. A. Ibrahim, "A compact double-sided MIMO antenna with an improved isolation for UWB applications," *Aeu-international Journal of Electronics and Communications*, Vol. 82, 7–13, 2017.

[22] Khan, A. A., S. A. Naqvi, M. S. Khan, and B. Ijaz, "Quad port miniaturized MIMO antenna for uwb 11 GHz and 13 GHz frequency bands," *AEU — International Journal of Electronics and Communications*, Vol. 131, 153618, 2021.

[23] Ban, Y.-L., Z.-X. Chen, Z. Chen, K. Kang, and J. L.-W. Li, "Decoupled hepta-band antenna array for WWAN/LTE smartphone applications," *IEEE Antennas and Wireless Propagation Letters*, Vol. 13, 999–1002, 2014.

[24] Liu, Y., X. Yang, Y. Jia, and Y. J. Guo, "A low correlation and mutual coupling MIMO antenna," *IEEE Access*, Vol. 7, 127 384–127 392, 2019.

[25] Sahu, N. K., G. Das, and R. K. Gangwar, "Dual polarized triple-band dielectric resonator based hybrid MIMO antenna for WLAN/WIMAX applications," *Microwave and Optical Technology Letters*, Vol. 60, No. 4, 1033–1041, 2018.

[26] Manteghi, M. and Y. Rahmat-Samii, "Multiport characteristics of a wide-band cavity backed annular patch antenna for multipolarization operations," *IEEE Transactions on Antennas and Propagation*, Vol. 53, No. 1, 466–474, 2005.

[27] Fritz-Andrade, E., H. Jardon-Aguilar, and J. A. Tirado-Mendez, "The correct application of total active reflection coefficient to evaluate MIMO antenna systems and its generalization to N ports," *International Journal of RF and Microwave Computer-aided Engineering*, Vol. 30, No. 4, e22113, 2020.

[28] Sultan, K. S. and H. H. Abdullah, "Planar UWB MIMO-diversity antenna with dual notch characteristics," *Progress In Electromagnetics Research C*, Vol. 93, 119–129, 2019.

[29] Yun, J. X. and R. G. Vaughan, "Multiple element antenna efficiency and its impact on diversity and capacity," *IEEE Transactions on Antennas and Propagation*, Vol. 60, No. 2, 529–539, 2011.

[30] Zhao, A. and Z. Ren, "Wideband MIMO antenna systems based on coupled-loop antenna for 5G N77/N78/N79 applications in mobile terminals," *IEEE Access*, Vol. 7, 93 761–93 771, 2019.